frontiers | Frontiers in Materials

ORIGINAL RESEARCH
published: 21 June 2022
doi: 10.3389/fmats.2022.941395

# Compact Fano-Type Liquid Metamaterial Resonator for High-Precision Temperature Sensing

*Haotian Chen**

*School of Sciences, Southwest Petroleum University, Chengdu, China*

In this paper, a liquid metal mercury (Hg) based high quality-factor (Q-factor) liquid electromagnetic metamaterial unit, the Hg Fano resonator, is designed for the high-precision temperature sensing application. Such Fano resonance in the Hg-resonator is excited by the microstrip-line coupling and the resonance frequency is sensitive to the background temperature changes. Based on the high Q-factor and the temperature-sensitive features of Hg-Fano resonator, the high-precision temperature sensing performance is discussed and achieved, with numerical and experimental demonstrations. The experimental sensitivity of 11.7 MHz/°C and figure-of-merit (FOM) of 0.4/°C are obtained. The proposed compact Hg-Fano resonator-based sensor can be widely used for the wireless temperature sensing area.

**Keywords: fano-type resonator, liquid metal Hg, metamaterial unit, temperature sensing, high-precision**

OPEN ACCESS

***Edited by:***
*Ke Chen,*
*Nanjing University, China*

***Reviewed by:***
*Yongjun Huang,*
*University of Electronic Science and Technology of China, China*
*Guowen Ding,*
*Nanjing University of Information Science and Technology, China*
*Weiren Zhu,*
*Shanghai Jiao Tong University, China*

***Correspondence:**
*Haotian Chen*
*joyhaotian@163.com*

***Specialty section:***
*This article was submitted to Metamaterials, a section of the journal Frontiers in Materials*

***Received:*** *11 May 2022*
***Accepted:*** *25 May 2022*
***Published:*** *21 June 2022*

***Citation:***
*Chen H (2022) Compact Fano-Type Liquid Metamaterial Resonator for High-Precision Temperature Sensing. Front. Mater. 9:941395. doi: 10.3389/fmats.2022.941395*

## 1 INTRODUCTION

Sensors based on the novel electromagnetic structures, including dielectric resonators (Iqbal et al., 2019; Zhang et al., 2020a; Omer et al., 2020), parity-time (PT) symmetry structures (Zhang and Fang, 2018; Farhat et al., 2020; Cheng et al., 2021), carbon nanotubes (Camilli and Passacantando, 2018; Han et al., 2019), and micro-ring and nanobeam resonators (Wang et al., 2018; Xu et al., 2020), have been widely discussed and developed in recent years, to achieve the high sensitivity, high precision, and wide dynamical range performances. Those proposed various electromagnetic structure-based sensors have the abilities for the sensing and detecting of various physical (Wang et al., 2018; Zhang et al., 2020a; Farhat et al., 2020; Omer et al., 2020; Xu et al., 2020), and chemical (Zhang and Fang, 2018; Han et al., 2019; Iqbal et al., 2019) parameters. With the well-developed electromagnetic metamaterial techniques (Fernandez-Corbaton et al., 2019; Kadic et al., 2019; Zhang et al., 2020b; Cao et al., 2021), the new high-performance sensing methods based on the electromagnetic metamaterials, such as the resonate-type unit, transmission lines, and electromagnetic bandgap (EBG) structure, are widely discussed as well (Kabashin et al., 2009; Zhang et al., 2018a; Vivek et al., 2018; Gil et al., 2019; Jun et al., 2019; Yoo and Park, 2019; Mayani et al., 2020; Yao et al., 2021), because of the strong electro-magnetic resonance features of the metamaterial units and the high-sensitivity of resonance feature (including the resonance frequency and resonance amplitude) on the background environment changings. Also, it has been reported that various environment physical, chemical, or biomedical parameters changings will lead to changings in the permittivity or refractive index of substrates/superstrates which used to form the metamaterial units (Melik et al., 2009; Kairm et al., 2014; Liu et al., 2018; Azab et al., 2021; Bhardwaj et al., 2021). For example, the refractive index of the medium around the electromagnetic metamaterial unit will be altered with the changings of lesion and chemical composition/concentration, and by detecting and analyzing the changes of the electromagnetic wave transmission/reflection intensity or the shift of resonance frequency caused by

the corresponding refractive index various, the lesion and chemistry densities can be determined (Liu et al., 2018). Moreover, the relative position varying of the dielectric material around the metamaterial resonant unit will also result in changes in the equivalent refractive index of the surrounding dielectric material. Therefore, when forces with different intensities act on the electromagnetic metamaterial, the resonance frequency/intensity will be changed and thereby the force magnitude characteristics can be determined by the detected resonance frequency/intensity changes (Melik et al., 2009). Moreover, O. Karim et al. designed a closed-ring resonator (CRR) and a variety of open-ring resonators based on lithium niobate (LiNbO3) temperature-sensitive dielectric substrate and compared their respective temperature sensitivity performances (Kairm et al., 2014). This CRR structure-based sensor has a temperature sensitivity up to 7.286 MHz/°C.

Based on the above-mentioned basic principle demonstrations of the metamaterial-based sensing techniques, the practical compact metamaterial-inspired wireless sensors are also reported in recent years (Jun et al., 2019; Arif et al., 2020). However, most of the above-mentioned sensing mechanisms are based on the dielectric permittivity and/or refractive index changings of the surrounding materials. The sensing sensitivity performance is limited somehow. Furthermore, the conventional metamaterial-inspired sensors suffered from the low Q-factor and low figure-of-merit (FOM), resulting in the low sensing precision. And most importantly, with the permittivity and/or refractive index changings the dielectric loss is varied as well, leading to further deterioration in sensing precision (Kairm et al., 2014).

Recently, on the other hand, the liquid metal-based metamaterial including the conventional split ring resonator (SRR) (Kasirga et al., 2009), Omega-type resonator (Wang et al., 2013), C-shaped resonator (Liu et al., 2015), and cross ring-shaped resonator (Ling et al., 2015) are reported based on the Hg, EGaIn, and/or Galinstan, and the initial temperature sensing application based on the liquid metal-inspired metamaterial unit has been proposed (Ma et al., 2021). Moreover, several high-Q resonators have been developed at the same time, including the Fano (Fedotov et al., 2007; Zhang et al., 2018b), toroidal (Kaelberer et al., 2010; Liu et al., 2017), anapole (Miroshnichenko et al., 2015; Basharin et al., 2017; Wu et al., 2018; Savinov et al., 2019), and hybrid plasmonic (Zhang et al., 2020c) resonators and parts of those high-Q resonators have been proposed to achieve high-precision sensing in rectangular waveguide system (Ma et al., 2021; Li et al., 2022). In this paper, therefore, we propose a new high-Q Fano resonator based on the liquid metal Hg to realize the high-temperature sensitivity and fine sensing precision. Importantly, to simplify and miniaturize the electromagnetic wave and metamaterial unit coupling system, the microstrip coupling line is used to excite the Fano resonance. Different from the conventional metamaterial-inspired temperature sensors based on the surrounding dielectric medium properties changings, the proposed liquid metal-based high-Q Fano resonator temperature sensor is based on the natural large temperature sensitivity (large thermal expansion rate) of liquid metals, making the resonance of the Fano resonator highly-related to the temperature and leading to the large sensing sensitivity and precision performances. At the same time, the Fano resonant strength with almost unchanged Q-factor and FOM can be obtained. Therefore, it has many advantages compared to conventional solid-state metamaterial-inspired sensors.

# 2 STRUCTURE DESIGN AND NUMERICAL DEMONSTRATION

## 2.1 Basic Unit Design

The proposed new Fano resonator based on the liquid metal Hg is shown in **Figure 1B**. As can be seen, based on the basic operating and realization mechanism of Fano resonance (Kabashin et al., 2009; Yoo and Park, 2019) (see **Figure 1A**), one asymmetric circular C-shaped Hg-ring with a different-height Hg-cylinder is placed inside a low-loss rectangular glass box ($\varepsilon_r$ = 3.7, tan$\delta$ = 0.0001). With $x$-polarization setting, the Hg-Fano resonator has asymmetric resonance feature theoretically (Kabashin et al., 2009; Yoo and Park, 2019), so the high Q-factor resonance can be excited. Moreover, different from the conventional Fano resonator, the additional Hg-cylinder is integrated into the asymmetric Hg-ring to achieve the large Hg-bar length changings when the background temperature is altered. This is mainly based on the natural temperature expansion property of Hg with the constant expansion rate of,

$$\gamma = (1/V_0) \cdot (\Delta V/\Delta T) \tag{1}$$

in a wide temperature varying range. Here $V_0$ is the initial total volume of the Hg-cylinder and Hg-ring without temperature changings, $\Delta V$ is the volume changing amount at the temperature changing $\Delta T$.

Based on the above-discussed design, the transmission curves with asymmetric Fano resonance features are firstly numerically modeled in finite element method based software. In simulations, the electromagnetic wave is incident along $z$-axis with the electric field along $x$-axis. The boundaries along the $x$ and $y$ direction are set as period. After simple structure optimization, the initial parameters for the designed Hg-Fano resonator is: $a$ = 0.4 mm, $h$ = 10 mm, $r_a$ = 10 mm, $r_m$ = 5 mm, $\theta_0$ = 40 deg, and the corresponding transmission ($|S_{21}|$) curves are shown in **Figure 1C**.

As can be seen, the asymmetric transmission feature is appeared at each curve, indicating the Fano resonance is achieved. Moreover, as shown in the inset of **Figure 1C** the obtained surface current distributions also indicate the asymmetric feature. Under different parameter $\theta$ values, the asymmetric transmission features are kept well. **Figures 1D,E** show the simulated Q-factor values, the calculated Fano resonance frequency shift, and the sensitivity for the proposed Hg-Fano resonator under different temperature changings. The represented temperature changings shown in **Figure 1** are calculated based on the expansion rate of Hg and the designed Hg-Fano resonator con-figuration,

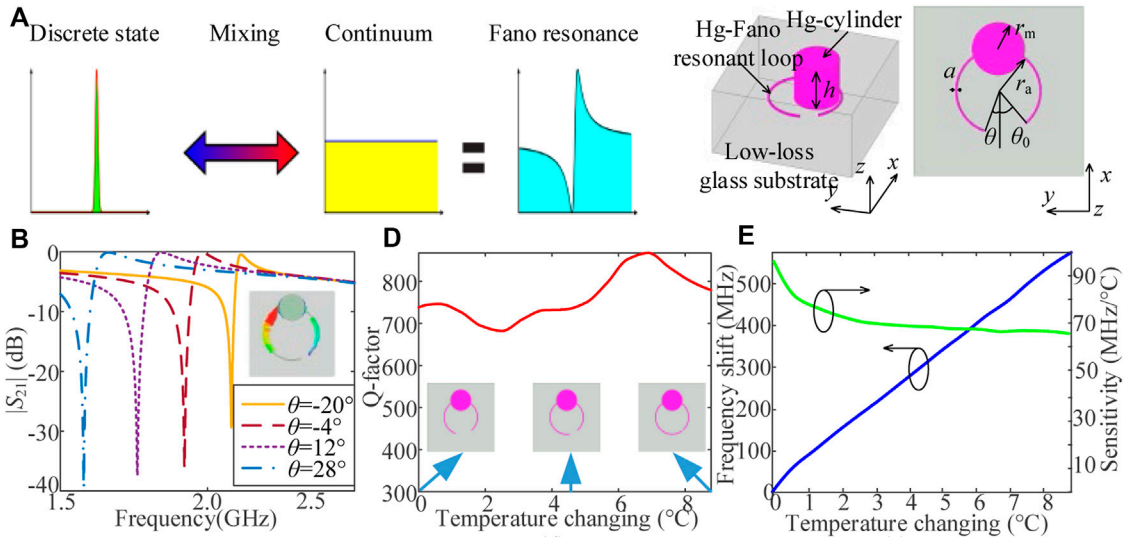


**FIGURE 1 | (A)** Theoretical presentation of the Fano resonance, **(B)** the 3D/2D view of the designed Hg-Fano resonator with parameter definitions, **(C)** transmission curves of the Hg-Fano resonator under different parameter $\theta$ values obtained by numerical simulation in the period boundary condition, and **(D,E)** the calculated Q-factor, resonant frequency shift, and temperature sensing sensitivity as a function of temperature changings. The modeled surface current distributions at Fano resonance frequency are shown in the inset in panel of **(C)**.

$$\Delta l = \frac{\Delta V}{a^2} = \frac{\gamma \cdot V_0 \cdot \Delta T}{a^2}, \tag{2}$$

where

$$V_0 = \pi r_m^2 \cdot h + 2\pi r_a \cdot a^2 \cdot \left(\frac{320 + \theta - 4\arcsin(r_m/r_a)}{360}\right), \tag{3}$$

Based on the basic resonance mechanism of the electromagnetic resonator, the resonance frequency is inversely related to the electric length (and results in the equivalent lumped parameter) of the resonator,

$$\omega = \sqrt{\frac{1}{(L_{\Delta T} + L_0)(C_{\Delta T} + C_0)}}, \tag{4}$$

here $L$ and $C$ are the equivalent inductance and capacitance. It shows that the proposed Hg-Fano resonator has a high stable Q-factor (around 750), and near-linear resonance frequency change features with quasi-constant sensitivity (~70 MHz/°C) under different temperature changings. The temperature sensing precision can be represented by the so-called figure-of-merit (FOM), in terms of (Zhang et al., 2020c),

$$\text{FOM} = \frac{\text{Sensitivity (MHz/°C)}}{\text{3dB} - \text{Bandwidth (MHz)}}. \tag{5}$$

And the FOM for this proposed Hg Fano resonator is calculated as about 26.25/°C, based on the results shown in **Figure 1**, which is much larger than most of the resonant-type temperature sensors (Kairm et al., 2014; Ma et al., 2021). Therefore, it can be considered as an ideal temperature sensing platform.

## 2.2 Microstrip-Line Coupling

The above obtained basic Hg Fano resonator is hard to be used as the temperature sensor node because of the electromagnetic excitation and coupling problems. Therefore, to solve this problem, in this section the microstrip-line is used and the proposed coupling mechanism is shown in **Figure 2A**. The circular loop is moved to the bottom of the Hg-cylinder to achieve good coupling between the microstrip-line and the resonator. Moreover, in this section, the Hg-cylinder size is reduced slightly and the final temperature sensitivity will be smaller than the one obtained in the previous section based on the theoretical relationship (see **Eq. 1**).

In the simulation for this microstrip-line coupling configuration, the radiation boundaries are applied to the glass box and two wave ports are excited along the microstrip-line, as shown in **Figure 2A**. The new parameter $r_m$ = 3 mm, $b$ = 1.13 mm, and the other structural parameters are not changed. The dielectric substrate (brown) of the microstrip line is the Rogers 4,350 ($\varepsilon_r$ = 3.66, tan$\delta$ = 0.004). Based on the above settings, the parallel results are concluded in **Figures 2B–D**. As can be seen in **Figure 2B**, the asymmetric transmission feature is kept with also high Q-factor values (about 180) under different temperature changing ranges. Compared to the results shown in **Figure 1C**, the reduced Q-factor values are mainly due to the radiation loss here because of the open radiation boundaries. However, the obtained Fano resonance frequency-changing features cannot keep the linear feature anymore, as shown in **Figure 1D**. This is because the coupling between the microstrip and the circular loop affects the resonance slightly. And the obtained average sensitivity is slightly smaller than the one shown in the **Figure 1D**, due to the reduced Hg-cylinder size as mentioned before. Moreover, the FOM for this microstrip-line coupled Hg

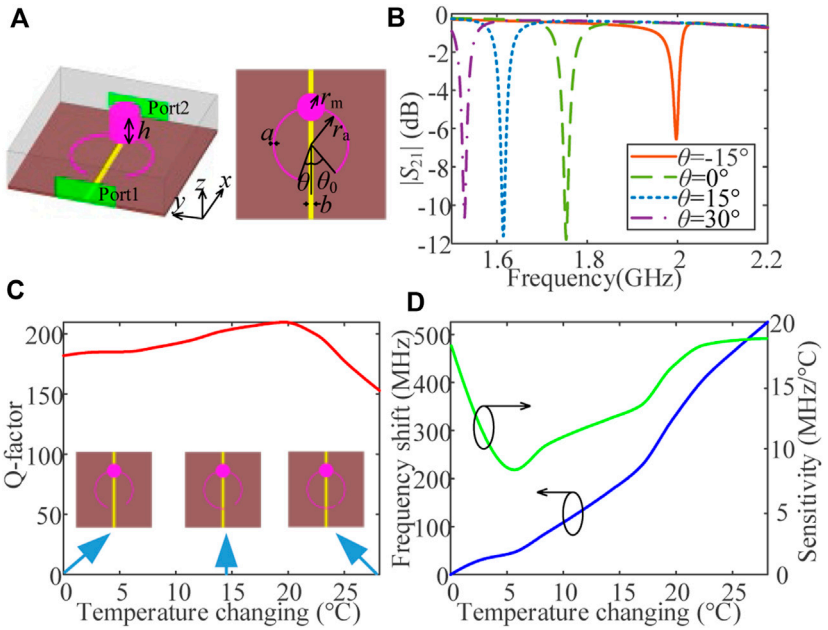


**FIGURE 2 | (A)** 3D view of the microstrip-line coupled Hg-Fano resonator with port setting in modeling environment and top view with parameters definition, **(B)** numerical transmission curves under different parameter $\theta$ values, and **(C,D)** the calculated Q-factor, resonant frequency shift, and temperature sensing sensitivity as a function of temperature changings.

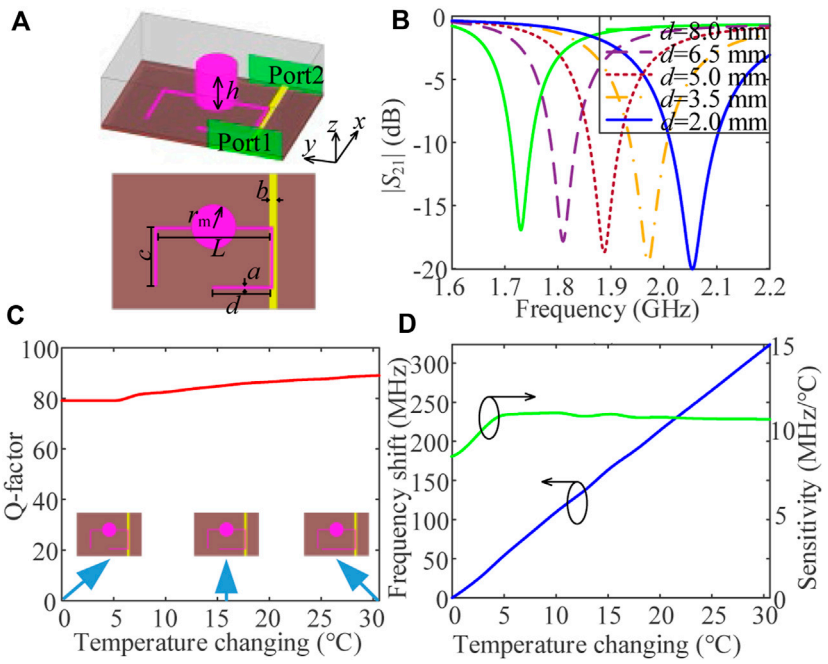


**FIGURE 3 | (A)** 3D view of the modified Hg-Fano resonator with port setting in modeling environment and top view with parameters definition, **(B)** numerical transmission curves under different parameter d values, and **(C,D)** the calculated Q-factor, resonant frequency shift, and temperature sensing sensitivity as a function of temperature changings.

Fano resonator is about 1.5/°C, smaller than the one shown in previous subsection.

## 2.3 Modified Hg-Fano Resonator

To achieve the near-linear Fano resonance frequency-changing feature with the constant sensitivity for future temperature sensing applications, in this subsection a modified Hg Fano resonator configuration is proposed, as shown in **Figure 3A**. As can be seen, the circular loop is changed to a rectangular loop, and the other structure configurations are not changed. Based on the similar optimization process the new structural parameters are obtained as: $a$ = 0.4 mm, $L$ = 15.2 mm, $c$ = 8.4 mm, $h$ = 6 mm, and $r_m$ = 3 mm. And the simulated parallel results are presented in **Figures 3B–D**. Compared to the previous two Fano resonators we have discussed, the Q-factor and sensitivity for this rectangular-shape Hg Fano resonator are further reduced due to the wide gap and shorter Hg-cylinder tank as shown in **Figure 3A**. However, here the more stable Q-factor (about 85), and near-liner Fano resonance frequency changes with near-constant sensitivity (~10 MHz/°C) are obtained. This is a benefit of the stable coupling strength between the microstrip-line and the resonator, because of that the rectangular shape resonator can make the Hg bar has a stronger and more stable coupling rate to the microstrip-line, as shown in **Figure 3A**. In the next section, the temperature sensing performance for the last discussed Hg Fano resonator is experimentally demonstrated.

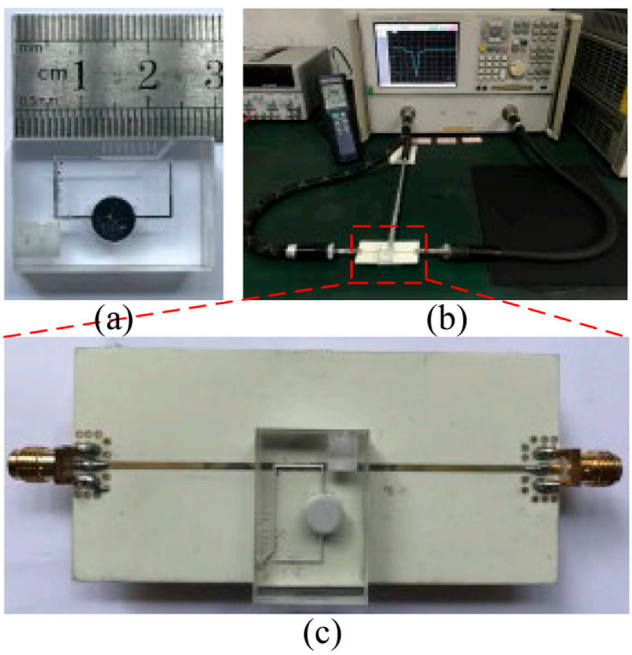


**FIGURE 4 | (A)** Fabricated rectangular-shape Hg Fano resonator prototype, **(B)** prepared whole measurement setup for the temperature sensing performance demonstration, and **(C)** zoomed in plot for the prototype over the microstrip line.

# 3 EXPERIMENTAL DEMONSTRATIONS

To fabricate the designed Hg Fano resonator prototype, one low-loss silica glass with good transparency is used as the substrate, and the hollow pile and cylinder tank which are used to store the liquid metals Hg are machined on the substrate with a precision laser etching technique. Then, one thin additional silica glass cover plate is placed on the etched glass substrate and such to glass are stuck tightly by using the UV glue. In the etching process, in order to inject the Hg into the fabricated hollow pile and the cylinder tank to form the rectangular Hg Fano resonator, a through-hole beside the hollow pile is also etched. Finally, the Hg is injected into the whole hollow pile and cylinder tank by using a syringe, and the achieved rectangular Hg Fano resonator prototype is shown in **Figure 4A**. It should be noticed that the size of the fabricated prototype and the used silica glass are the same as used in numerical simulations in the previous section. One big hole on the left side of the glass box as shown in **Figure 4A** is used to place the commercial thermometer probe, as shown in the whole measurement setup (**Figure 4B**). The final assembled Hg Fano resonator is placed on the top of a pre-fabricated 50-Ω straight microstrip-line with the optimized position shown in **Figures 3A**, **4C**.

In the real-time measurement, the background temperature around the Hg Fano resonator is controlled by a heater and is monitored by the commercial thermometer shown in **Figure 4B**. Moreover, for a regular S-parameter measurement procedure, the two ports of the vector network analyzer (Agilent 5230A) with the reference plane reaching the two SMA connectors are calibrated by the regular TRL calibration procedure process.

Then the transmission curves are collected in real time under different background temperatures ranging from 26 to 38°C with changing step of 0.1°C, and the measured two-dimensional results are presented in **Figure 5A**. Several transmission curves at different temperature points are also shown in **Figure 5B** to see the asymmetric transmission shape, and the calculated Q-factor and the collected Fano resonance frequency shift as a function of temperature are concluded in **Figures 5C,D**, respectively. It can be found that the fabricated Hg Fano resonator coupled by the microstrip-line still shows the asymmetric Fano transmission shape with the Q-factor around 70, and the Fano resonance frequency is almost linear shifted when the temperature is increased gradually indicating a calculated sensitivity of 11.7 MHz/°C, and FOM of 0.4/°C. Those obtained measurement results agree well to the corresponding numerical results shown in **Figure 3**. The slight reduction for the Q-factor is because of the in-perfect sample fabrication, glass pasting, and placing processes. Moreover, the dielectric loss of the practical glass and the invasion of the commercial thermometer probe closed to the Hg Fano resonator will also result in the reduction of the resonance strength and Q-factor.

However, the measured sensitivity is slightly larger than the simulated one. This is due to the fact that the initial Hg volume $V_0$ is hard to control finely and equal to the numerical one. So the larger sensitivity is reasonable. This is also one theoretical direction for enhancing the sensitivity and FOM by enlarging

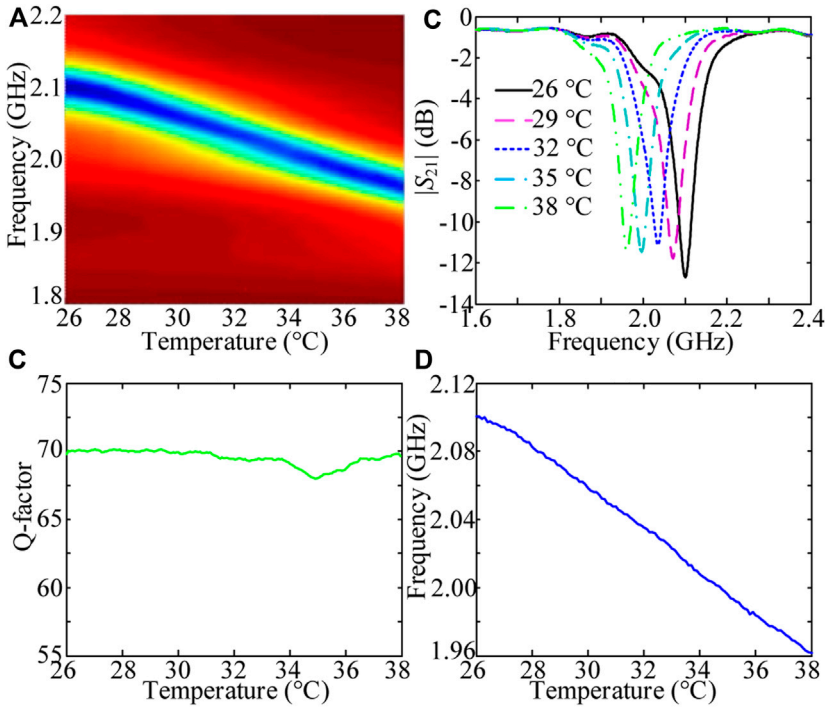


**FIGURE 5 | (A)** Two-dimensional sweep of the transmission curves under different temperatures, **(B)** the selected several transmission curves at the temperatures shown in the inset, **(C,D)** the calculated Q-factor and the collected resonance frequency shift as a function of temperature.

**TABLE 1 |** Performance comparisons of different kind of temperature sensors.

| Works | Sensing Mechanism | Unit Dimension (with Coupling system) | Sensitivity | FOM |
|---|---|---|---|---|
| Kairm et al. (2014) | Dielectric constant changing of the CRR resonator | — | 7.3 MHz/°C[a] | — |
| Ma et al. (2021) | Thermal expansion of Hg toroidal resonator in waveguide | 110 × 55 × 200 mm | 16.4 MHz/°C | 0.59/°C |
| Li et al. (2022) | Thermal expansion of Hg EIT resonator in waveguide | 72 × 34 × 120 mm | 9.5 MHz/°C | 0.68/°C |
| Haitao Cheng et al. (2012) | Dielectric constant changing of the antenna substrate | 47 × 22 × 50 mm | 0.4 MHz/°C | 0.016/°C |
| Lorenzo et al. (2016) | RFID tag with NTC thermistor | 26 × 72×5 mm | 0.23 kHz/°C | – |
| This work | Thermal expansion of Hg Fano resonator over microstrip line | 7 × 60 × 100 mm | 11.7 MHz/°C | 0.4/°C |

[a]*Simulation results.*

the initial Hg volume based on the theoretical equations and the numerical results shown in **Section 2.1**.

Finally, the temperature sensing performances and dimensions for the designed microstrip-line coupled Hg Fano resonator are compared with the previously reported temperature sensors based on other antenna and metamaterial techniques (Haitao Cheng et al., 2012; Kairm et al., 2014; Lorenzo et al., 2016; Li et al., 2022). As can be seen in **Table 1**, most of the reported microwave temperature sensors are realized by using the temperature-sensitive dielectrics as the substrate of antennas and/or metamaterial resonator units. And those works did not investigate the method to enhance the resonance Q-factor. So both the sensing sensitivity and precision cannot reach an optimized value. The proposed liquid metal Hg-based metamaterial resonator units, including the reported toroidal and EIT resonators realized in the waveguide (Ma et al., 2021; Li et al., 2022) and the one discussed in this paper coupled by the microstrip-line, can exhibit both the high Q-factor and high-temperature sensing performances, because that the Hg is directly used to design the resonators, not just the substrates. Those are the main advantages compared with the previously reported metamaterial-inspired microwave temperature sensors. Moreover, even though the Hg toroidal and EIT resonators showed slightly larger sensitivity and FOM, however, it is realized in a bulk waveguide which is hard to use in practical application. Therefore, the discussed microstrip-line coupled Hg Fano resonator shown in this paper with compact size can be widely used for the wireless temperature sensing area in the near future.

As obtained in this paper, both the simulated and simulated Fano resonant frequency shift is kept well as a near-linear feature. This is mainly because of that in this limited temperature

increasing range, the Hg bar length is not changed too much so the Fano resonant feature can be kept well, and the resonant frequency is linearly related to the temperature. However, there is an upper limit that can make the linear frequency shift property not be satisfied anymore. When the changeable Hg bar is closed to the other Hg bar as shown in **Figure 3A** because of the continuing increase of temperature, the Fano resonance will disappear. So in that case, the high-performance sensing property cannot be kept.

## 4 CONCLUSION

In this paper, a Hg Fano resonator coupled with the microstrip-line is designed for microwave high-precision temperature sensing applications. With detailed Fano resonator evolution, and the numerical and experimental demonstrations, the measured sensitivity of 11.7 MHz/°C and FOM of 0.4/°C are obtained, and such temperature sensing performances can be further enhanced by simply enlarging the initial Hg volume for the Fano resonator structure. The proposed microstrip-line coupled Hg Fano resonator can be widely used for the wireless temperature sensing area.

## DATA AVAILABILITY STATEMENT

The original contributions presented in the study are included in the article/supplementary material, further inquiries can be directed to the corresponding author.

## AUTHOR CONTRIBUTIONS

HC proposed the research idea, finished the numerical simulation and experimental analysis, and finished the whole manuscript writing and finalization.

## REFERENCES


Arif, A., Zubair, A., Riaz, K., Mehmood, M. Q., and Zubair, M. (2020). A Novel Cesaro Fractal EBG-Based Sensing Platform for Dielectric Characterization of Liquids. *IEEE Trans. Antennas Propag.* 69 (5), 2887–2895. doi:10.1109/TAP.2020.3028201

Azab, M. Y., Hameed, M. F. O., Nasr, A. M., and Obayya, S. S. A. (2021). Highly Sensitive Metamaterial Biosensor for Cancer Early Detection. *IEEE Sensors J.* 21 (6), 7748–7755. doi:10.1109/jsen.2021.3051075

Basharin, A. A., Chuguevsky, V., Volsky, N., Kafesaki, M., and Economou, E. N. (2017). Extremely High Q-Factor Metamaterials Due to Anapole Excitation. *Phys. Rev. B* 95 (3), 035104. doi:10.1103/physrevb.95.035104

Bhardwaj, A., Pratap, D., Vaibhav Srivastava, K., and Ramakrishna, S. A. (2021). Highly Sensitive Permittivity Sensor Using an Inhomogeneous Metamaterial Cylindrical Waveguide. *IEEE Sensors J.* 21 (7), 9120–9127. doi:10.1109/jsen.2021.3050778

Camilli, L., and Passacantando, M. (2018). Advances on Sensors Based on Carbon Nanotubes. *Chemosensors* 6 (4), 62. doi:10.3390/chemosensors6040062

Cao, G., Xu, H.-X., Zhou, L.-M., Deng, Y., Zeng, Y., Dong, S., et al. (2021). Infrared Metasurface-Enabled Compact Polarization Nanodevices. *Mater. Today* 50, 499–515. doi:10.1016/j.mattod.2021.06.014

Cheng, J., Liu, D., Dong, P., Wang, G., Chi, F., and Liu, S. (2021). Photonic Spin Hall Effect in a Parity-Time Symmetric Cavity and its Sensing Application. *Opt. Commun.* 498, 127247. doi:10.1016/j.optcom.2021.127247

Farhat, M., Yang, M., Ye, Z., and Chen, P.-Y. (2020). PT-symmetric Absorber-Laser Enables Electromagnetic Sensors with Unprecedented Sensitivity. *ACS Photonics* 7 (8), 2080–2088. doi:10.1021/acsphotonics.0c00514

Fedotov, V. A., Rose, M., Prosvirnin, S. L., Papasimakis, N., and Zheludev, N. I. (2007). Sharp Trapped-Mode Resonances in Planar Metamaterials with a Broken Structural Symmetry. *Phys. Rev. Lett.* 99 (14), 147401. doi:10.1103/physrevlett.99.147401

Fernandez-Corbaton, I., Rockstuhl, C., Ziemke, P., Gumbsch, P., Albiez, A., Schwaiger, R., et al. (2019). New Twists of 3D Chiral Metamaterials. *Adv. Mater* 31 (26), e1807742. doi:10.1002/adma.201807742

Gil, M., Vélez, P., Aznar-Ballesta, F., Muñoz-Enano, J., and Martín, F. (2019). Differential Sensor Based on Electroinductive Wave Transmission Lines for Dielectric Constant Measurements and Defect Detection. *IEEE Trans. Antennas Propag.* 68 (3), 1876–1886. doi:10.1109/TAP.2019.2938609

Haitao Cheng, H., Ebadi, S., and Xun Gong, X. (2012). A Low-Profile Wireless Passive Temperature Sensor Using Resonator/Antenna Integration up to 1000${\circ}$C. *Antennas Wirel. Propag. Lett.* 11, 369–372. doi:10.1109/lawp.2012.2192249

Han, T., Nag, A., Chandra Mukhopadhyay, S., and Xu, Y. (2019). Carbon Nanotubes and its Gas-Sensing Applications: A Review. *Sensors Actuators A Phys.* 291, 107–143. doi:10.1016/j.sna.2019.03.053

Iqbal, A., Smida, A., Saraereh, O., Alsafasfeh, Q., Mallat, N., and Lee, B. (2019). Cylindrical Dielectric Resonator Antenna-Based Sensors for Liquid Chemical Detection. *Sensors* 19 (5), 1200. doi:10.3390/s19051200

Jun, S. Y., Sanz Izquierdo, B., and Parker, E. A. (2019). Liquid Sensor/detector Using an EBG Structure. *IEEE Trans. Antennas Propagat.* 67 (5), 3366–3373. doi:10.1109/tap.2019.2902663

Kabashin, A. V., Evans, P., Pastkovsky, S., Hendren, W., Wurtz, G. A., Atkinson, R., et al. (2009). Plasmonic Nanorod Metamaterials for Biosensing. *Nat. Mater* 8 (11), 867–871. doi:10.1038/nmat2546

Kadic, M., Milton, G. W., van Hecke, M., and Wegener, M. (2019). 3D Metamaterials. *Nat. Rev. Phys.* 1 (3), 198–210. doi:10.1038/s42254-018-0018-y

Kaelberer, T., Fedotov, V. A., Papasimakis, N., Tsai, D. P., and Zheludev, N. I. (2010). Toroidal Dipolar Response in a Metamaterial. *Science* 330 (6010), 1510–1512. doi:10.1126/science.1197172

Kairm, H., Delfin, D., Shuvo, M. A. I., Chavez, L. A., Garcia, C. R., Barton, J. H., et al. (2014). Concept and Model of a Metamaterial-Based Passive Wireless Temperature Sensor for Harsh Environment Applications. *IEEE Sensors J.* 15 (3), 1445–1452. doi:10.1109/JSEN.2014.2363095

Kasirga, T. S., Ertas, Y. N., and Bayindir, M. (2009). Microfluidics for Reconfigurable Electromagnetic Metamaterials. *Appl. Phys. Lett.* 95 (21), 214102. doi:10.1063/1.3268448

Li, J., Zhou, Y., Peng, F., Chen, D., Xian, C., Kuang, P., et al. (2022). High-FOM Temperature Sensing Based on Hg-EIT-like Liquid Metamaterial Unit. *Nanomaterials* 12 (9), 1395. doi:10.3390/nano12091395

Ling, K., Kim, K., and Lim, S. (2015). Flexible Liquid Metal-Filled Metamaterial Absorber on Polydimethylsiloxane (PDMS). *Opt. Express* 23 (16), 21375–21383. doi:10.1364/oe.23.021375

Liu, P., Yang, S., Jain, A., Wang, Q., Jiang, H., Song, J., et al. (2015). Tunable Meta-Atom Using Liquid Metal Embedded in Stretchable Polymer. *J. Appl. Phys.* 118 (1), 014504. doi:10.1063/1.4926417

Liu, Y., Zhan, S., Cao, G., Li, J., Yang, H., Liu, Q., et al. (2018). Theoretical Design of Plasmonic Refractive Index Sensor Based on the Fixed Band Detection. *IEEE J. Sel. Top. Quantum Electron.* 25 (2), 1–6. doi:10.1109/JSTQE.2018.2827661

Liu, Z., Du, S., Cui, A., Li, Z., Fan, Y., Chen, S., et al. (2017). High-Quality-Factor Mid-Infrared Toroidal Excitation in Folded 3D Metamaterials. *Adv. Mat.* 29 (17), 1606298. doi:10.1002/adma.201606298

Lorenzo, J., Lazaro, A., Villarino, R., and Girbau, D. (2016). Modulated Frequency Selective Surfaces for Wearable RFID and Sensor Applications. *IEEE Trans. Antennas Propagat.* 64 (10), 4447–4456. doi:10.1109/tap.2016.2596798

Ma, L., Chen, D., Zheng, W., Li, J., Wang, W., Liu, Y., et al. (2021). Thermally Tunable High-Q Metamaterial and Sensing Application Based on Liquid Metals. *Opt. Express* 29 (4), 6069–6079. doi:10.1364/oe.418024

Mayani, M. G., Herraiz-Martínez, F. J., Domingo, J. M., and Giannetti, R. (2020). Resonator-based Microwave Metamaterial Sensors for Instrumentation: Survey, Classification, and Performance Comparison. *IEEE Trans. Instrum. Meas.* 70, 1–14. doi:10.1109/TIM.2020.3040484

Melik, R., Unal, E., Perkgoz, N. K., Santoni, B., Kamstock, D., Puttlitz, C., et al. (2009). Nested Metamaterials for Wireless Strain Sensing. *IEEE J. Sel. Top. Quantum Electron.* 16 (2), 450–458. doi:10.1109/JSTQE.2009.2033391

Miroshnichenko, A. E., Evlyukhin, A. B., Yu, Y. F., Bakker, R. M., Chipouline, A., Kuznetsov, A. I., et al. (2015). Nonradiating Anapole Modes in Dielectric Nanoparticles. *Nat. Commun.* 6 (1), 8069–8078. doi:10.1038/ncomms9069

Omer, A. E., Shaker, G., Safavi-Naeini, S., and Shubair, R. (2020). Multiple-cell Microfluidic Dielectric Resonator for Liquid Sensing Applications. *IEEE Sensors J.* 21 (5), 6094–6104. doi:10.1109/JSEN.2020.3041700

Savinov, V., Papasimakis, N., Tsai, D. P., and Zheludev, N. I. (2019). Optical Anapoles. *Commun. Phys.* 2 (1), 1–4. doi:10.1038/s42005-019-0167-z

Vivek, A., Shambavi, K., and Alex, Z. C. (2018). A Review: Metamaterial Sensors for Material Characterization. *Sens. Rev.* 39 (3), 417–432.

Wang, C., Fu, Z., Sun, F., Zhou, J., and Tian, H. (2018). Large-dynamic-range Dual-Parameter Sensor Using Broad FSR Multimode Photonic Crystal Nanobeam Cavity. *IEEE Photonics J.* 10 (5), 1–14. doi:10.1109/jphot.2018.2865510

Wang, J., Liu, S., Guruswamy, S., and Nahata, A. (2013). Reconfigurable Liquid Metal Based Terahertz Metamaterials via Selective Erasure and Refilling to the Unit Cell Level. *Appl. Phys. Lett.* 103 (22), 221116. doi:10.1063/1.4837675

Wu, P. C., Liao, C. Y., Savinov, V., Chung, T. L., Chen, W. T., Huang, Y.-W., et al. (2018). Optical Anapole Metamaterial. *ACS Nano* 12 (2), 1920–1927. doi:10.1021/acsnano.7b08828

Xu, Y., Hu, S., and Kong, M. (2020). Air-Mode Photonic Crystal Micro-Ring Resonator with Enhanced Quality Factor for Refractive Index Sensing. *IEEE Photonics J.* 12 (3), 1–11. doi:10.1109/jphot.2020.2993603

Yao, H., Mei, H., Zhang, W., Zhong, S., and Wang, X. (2021). Theoretical and Experimental Research on Terahertz Metamaterial Sensor with Flexible Substrate. *IEEE Photonics J.* 14 (1), 1–9. doi:10.1109/JPHOT.2021.3124414

Yoo, S., and Park, Q.-H. (2019). Metamaterials and Chiral Sensing: a Review of Fundamentals and Applications. *Nanophotonics* 8 (2), 249–261. doi:10.1515/nanoph-2018-0167

Zhang, J., Chen, Z., Cao, J., Huang, C., and Tian, G. (2020). A Cylindrical Ring Dielectric Resonator Based Passive Wireless Sensor for Position Insensitive Crack Monitoring. *Sensors Actuators A Phys.* 316, 112420. doi:10.1016/j.sna.2020.112420

Zhang, T., Chen, X., Thakur, Y., Lu, B., Zhang, Q., Runt, J., et al. (2020). A Highly Scalable Dielectric Metamaterial with Superior Capacitor Performance over a Broad Temperature. *Sci. Adv.* 6 (4), eaax6622. doi:10.1126/sciadv.aax6622

Zhang, X., Yan, R. T., and Cui, T. J. (2020). High-FoM Resonance in Single Hybrid Plasmonic Resonator via Electromagnetic Modal Interference. *IEEE Trans. Antennas Propagat.* 68 (8), 6447–6451. doi:10.1109/tap.2020.2970037

Zhang, Y. C., and Fang, Y. T. (2018). Gas Sensor Based on Parity-Time-Symmetry Structure. *J. Nanophot.* 12 (3), 036005. doi:10.1117/1.jnp.12.036005

Zhang, Y., Liu, W., Li, Z., Li, Z., Cheng, H., Chen, S., et al. (2018). High-quality-factor Multiple Fano Resonances for Refractive Index Sensing. *Opt. Lett.* 43 (8), 1842–1845. doi:10.1364/ol.43.001842

Zhang, Z., Zhou, J., Littlejohns, C. G., Reed, G. T., Wang, H., Ng, G. I., et al. (2018). Mid-infrared Sensor Based on a Suspended Microracetrack Resonator with Lateral Subwavelength-Grating Metamaterial Cladding. *IEEE Photonics J.* 10 (2), 1–8. doi:10.1109/jphot.2018.2809662

**Conflict of Interest:** The authors declare that the research was conducted in the absence of any commercial or financial relationships that could be construed as a potential conflict of interest.

**Publisher's Note:** All claims expressed in this article are solely those of the authors and do not necessarily represent those of their affiliated organizations, or those of the publisher, the editors and the reviewers. Any product that may be evaluated in this article, or claim that may be made by its manufacturer, is not guaranteed or endorsed by the publisher.